Thermo-Economic Analysis of a Solar Flat Plate Collector-Driven HDH Desalination System for Arid Coastal Regions of Pakistan

Sadam Hussain Soomro[1, *], Imran Mir Chohan[2], Afsheen Sheikh[3], Asif Ahmed Jogi[2]
[1]Department of Mechanical Engineering Technology, The Benazir Bhutto Shaheed University of Technology and Skill Development, Khairpur Mirs 66020, Sindh, Pakistan
[2]Department of Mechanical Engineering Technology, Indus University, Karachi 75300, Pakistan
[3]Department of Civil Engineering Technology, Indus University, Karachi 75300, Pakistan
*Corresponding Author: saddamarif7@gmail.com
Received: 01-05-2026, Received in Revised form: 29-05-2026, Accepted: 16-06-2026, Published: 30-06-2026

Abstract

Pakistan faces severe freshwater stress, particularly in arid coastal regions such as Gwadar, where conventional freshwater resources are limited, but seawater and solar energy are abundant. This study presents a numerical performance and economic assessment of a solar-driven humidification–dehumidification desalination system integrated with a flat plate collector under Gwadar's climatic conditions. Mathematical models of the collector and HDH subsystems were developed and solved in MATLAB to evaluate the effects of solar irradiance, ambient temperature, seawater inlet temperature, absorber and insulation materials, air mass flow rate, humidifier inlet water temperature, coolant temperature, and cooling-water flow rate. The results showed that Gwadar's summer climate is favorable for solar desalination, with peak irradiance of approximately 960 W/m² and ambient temperature reaching 39.2°C. The collector outlet temperature increased to about 90.1°C, while useful heat gain reached 0.66 kW. Copper absorber and polyurethane insulation provided the best thermal performance. Under favorable conditions, the system achieved a maximum freshwater productivity of 6.15 kg/h (4.10 kg m^{-2} h^{-1} based on the 1.5 m² collector area), a peak gain output ratio of 2.62, and a daily freshwater yield of approximately 34.5 kg. The levelized cost of water ranged from 18.0 PKR/L under conservative low-yield operation to approximately 1.34–4.0 PKR/L under improved production scenarios. Inflation analysis showed that higher inflation significantly increases long-term water costs. Model validation against published data produced average relative errors below 5%. Overall, the proposed system is technically feasible and economically promising for decentralized freshwater production in Gwadar and similar coastal regions.
Keywords: Humidification-dehumidification, Desalination, Flat-Plate-Collector, Solar Energy.

Introduction

Freshwater scarcity has become one of the most serious environmental and socio-economic challenges for arid and coastal regions. Although the Earth contains abundant water, only a very small fraction is directly suitable for domestic, agricultural, and industrial use. Rapid population growth, urbanization, climate variability, and the overexploitation of conventional freshwater resources have further increased the pressure on available water supplies. This problem is particularly critical in developing countries, where many coastal and remote communities still lack access to safe, reliable drinking water. Pakistan is also experiencing increasing water stress, and the situation is more difficult in arid coastal regions such as Gwadar, where freshwater resources are limited, and the demand for clean water is increasing due to population growth, port development, and expanding economic activities [1].

Desalination effectively converts saline or seawater into potable water. Existing desalination technologies are generally classified into membrane-based and thermal-based processes. Reverse osmosis (RO) and electrodialysis (ED) are the most common membrane-based technologies. Meanwhile, multi-stage flash distillation (MSF), multi-effect distillation (MED), and humidification–dehumidification (HDH) are major thermal desalination methods. RO is widely used because of its compactness and high salt rejection; however, it requires high-quality electrical energy, careful pretreatment, and regular membrane maintenance. MSF and MED are reliable for large-scale seawater desalination, but their high capital cost, large energy demand, and operational complexity limit their suitability for small and remote communities. Therefore, there is a strong need for simple, low-cost, and renewable-energy-driven desalination systems that can operate efficiently under local climatic conditions. Humidification–dehumidification desalination is considered a promising small-scale desalination technology because it follows the natural rain cycle. In the humidifier, hot saline water comes into direct contact with air, allowing the air to absorb moisture. The hot and humid air is then passed through a dehumidifier, where it is cooled, and the water vapor condenses as freshwater. The remaining brine is discharged separately. Compared with conventional thermal desalination processes, HDH systems are simpler in construction, easier to operate, and suitable for low-grade heat sources. Their performance depends strongly on air and water temperatures, air and water mass flow rates, humidifier and dehumidifier effectiveness, and thermal energy availability. These characteristics make HDH desalination especially suitable for solar-assisted operation in coastal and arid regions. Solar energy is one of the most attractive heat sources for HDH desalination because it is clean, abundant, and locally available in many water-scarce regions. Among solar thermal collectors, the flat plate collector (FPC) is simple, economical, and technically suitable for heating seawater to the moderate temperature range required by HDH systems. The heated seawater leaving the FPC can be supplied directly to the humidifier, where higher water temperature increases vapor pressure and enhances moisture transfer to the airstream. In coastal regions such as Gwadar, high solar radiation, warm ambient temperatures, and seawater availability create favorable conditions for solar-driven HDH desalination. Therefore, integrating an FPC with an HDH unit can provide a practical, sustainable solution for decentralized freshwater production.

http://dx.doi.org/10.24949/njes.v19i1.996

Several studies have investigated solar-assisted HDH desalination using different collector configurations and operating strategies. Santosh et al. reviewed solar-based HDH desalination systems. They reported that freshwater production depends mainly on air and water mass flow rates, inlet fluid temperatures, and solar radiation intensity. Their study also highlighted the potential of combining different types of solar collectors to improve overall HDH performance [2]. Mohamed et al. thermodynamically evaluated a solar HDH system integrated with a parabolic trough collector for air preheating. They found that freshwater production increased during summer due to higher solar radiation and longer sunshine duration [3]. Khalil et al. experimentally studied an HDH system equipped with a bubble-column humidifier and an evacuated tube collector. Their results showed improved humidification performance compared with conventional packed-bed humidifiers [4]. Yildirim et al. performed a parametric analysis of a dual-heating HDH system using a flat plate water collector and a double-pass solar air heater, concluding that simultaneous air and water preheating improved freshwater productivity [5]. Other researchers have also focused on improving the productivity and energy performance of solar HDH systems. Sharshir et al. developed a hybrid solar desalination unit combining HDH with solar stills. They reported significant improvement in gain output ratio and freshwater yield by reusing the residual heat of hot brine [6]. Antar and Sharqawy experimentally compared single-stage and two-stage air-heated HDH desalination systems and found that the two-stage configuration produced higher distillate output [7]. Further investigations on water-heated HDH systems showed that humidifier inlet water temperature, air mass flow rate, seawater mass flow rate, and the water-to-air mass flow ratio strongly influence freshwater productivity and system performance [8,9]. Additional studies using flat plate solar air heaters and hybrid water–air heating arrangements confirmed that solar radiation intensity and collector area play important roles in improving the thermal performance and freshwater production rate of HDH desalination systems [10–12]. The reviewed literature confirms that solar-assisted HDH desalination has considerable potential for decentralized freshwater production. However, most previous studies were conducted in climates outside Pakistan, and limited attention has been given to the performance of solar-driven HDH desalination under Gwadar's specific environmental conditions. Gwadar's solar radiation pattern, ambient temperature, wind speed, and seawater temperature can significantly influence the flat plate collector's thermal output and overall HDH cycle performance. Therefore, a location-specific performance assessment is necessary before recommending solar HDH desalination as a practical solution for this coastal region.

Although previous investigations have demonstrated the potential of solar-assisted humidification–dehumidification (HDH) desalination through different collector configurations, heating strategies, and system integration approaches, several research aspects remain insufficiently addressed, as illustrated in Table 1. Existing studies have examined parabolic trough collectors, evacuated tube collectors, flat plate collectors, solar air heaters, and hybrid heating arrangements, primarily focusing on improving thermal performance, freshwater productivity, and energy utilization. However, the performance of a simple flat plate collector-driven HDH desalination system under Gwadar's specific climatic conditions requires further investigation. The effectiveness of such a system is strongly influenced by local solar radiation, ambient temperature, seawater conditions, and the thermal characteristics of the collector components. Furthermore, the combined influence of absorber material, insulation material, air mass flow rate, seawater temperature, and humidifier operating conditions on the thermal and freshwater production performance of an FPC–HDH configuration has not been sufficiently explored for this geographical context. In addition, the economic implications of system productivity, capital investment, system lifetime, and inflation-sensitive water production costs require greater attention when evaluating the feasibility of decentralized solar desalination in coastal Pakistan.

Table 1: Comparison of Previous Studies with the Present Investigation

Previous studies	Main focus of cited studies	Distinction of the present work
Santosh et al. [2]	Reviewed solar-based humidification–dehumidification (HDH) desalination systems and discussed the effects of operating conditions, solar radiation, and collector integration.	The present study develops a location-specific numerical assessment of a flat plate collector (FPC)-assisted HDH system under the climatic conditions of Gwadar, Pakistan.
Mohamed et al. [3]	Investigated a solar HDH desalination system using a parabolic trough collector for air preheating and evaluated its thermodynamic performance.	The present work focuses on a simpler FPC-driven configuration and evaluates its thermal and freshwater production performance for a coastal region of Pakistan.
Khalil et al. [4]	Experimentally examined an HDH system incorporating a bubble-column humidifier and an evacuated tube solar collector to improve humidification.	The present study investigates the performance of an FPC-based HDH system and examines the effects of collector materials, insulation, and operating parameters.

NUST Journal of Engineering Sciences (NJES) is licensed under a Creative Commons Attribution 4.0 International License.

Previous studies	Main focus of cited studies	Distinction of the present work
Yildirim et al. [5]	Studied a dual-heating HDH configuration using a flat plate water collector and a double-pass solar air heater for simultaneous air and water heating.	Unlike the dual-heating arrangement, the present study evaluates an FPC-assisted HDH system while integrating thermal performance, freshwater productivity, and economic indicators.
Sharshir et al. [6]	Proposed a hybrid solar desalination system combining HDH desalination and solar stills, including the utilization of residual hot brine heat.	The present investigation concentrates on a comparatively simple FPC–HDH configuration intended for decentralized freshwater production without incorporating a solar still subsystem.
Antar and Sharqawy [7]	Compared single-stage and two-stage air-heated HDH systems and reported how multistage operation affects distillate production.	The present work evaluates a single FPC-assisted HDH arrangement under Gwadar-specific climatic conditions and emphasizes its practical thermal and economic feasibility.
Water-heated HDH studies from [8,9]	Investigated the effects of humidifier inlet water temperature, air mass flow rate, seawater flow rate, and water-to-air ratio on HDH performance.	This study integrates these operating parameters with solar radiation, ambient temperature, seawater inlet temperature, and collector-related properties in a unified MATLAB-based model.
Solar-assisted HDH studies [10–12]	Examined flat plate solar air heaters and hybrid air- and water-heating arrangements, highlighting the effects of solar radiation and collector area.	The present study combines FPC thermal analysis, HDH freshwater productivity, material selection, operating-parameter assessment, and water production cost under the environmental and economic conditions of Gwadar, Pakistan.

System Description

The proposed system mainly consists of two major parts: a Flat Plate Collector (FPC) and a Humidification–Dehumidification (HDH) desalination unit. The system is designed to use solar energy for heating seawater, which is then converted into fresh water through a humidification and condensation process. In this setup, seawater is first pumped from the sea and passed through a filter to remove any large impurities. The clean seawater then flows into the Flat Plate Collector (FPC), where it absorbs solar heat. The collector consists of an absorber plate made of a dark-colored metal (such as copper or aluminum) enclosed by a transparent glass cover. When sunlight falls on the collector, the absorber plate gets heated, and this heat is transferred to the flowing seawater inside the tubes. As a result, the water temperature increases, and the hot seawater leaves the collector and enters the humidifier. Inside the humidifier, the hot seawater is sprayed or made to flow over packing materials to increase the contact surface area between the air and water. Ambient air is passed through the humidifier, where it comes into direct contact with the hot seawater. During this process, the air absorbs moisture and becomes hot and humid. The remaining concentrated brine is safely discharged back to the sea or into a disposal tank. The hot, moist air from the humidifier then flows into the dehumidifier, where it comes into indirect contact with a stream of cool seawater flowing through tubes or fins. As the humid air cools down, water vapor condenses on the cold surfaces and forms fresh distilled water, which is collected in a freshwater tank. The air then leaves the system at a lower temperature and humidity level. This system is simple in design, easy to operate, and requires only low-grade solar heat. Because it does not depend on fossil fuels or high energy input, it is especially suitable for small communities in coastal and arid regions like Gwadar.

Methodology

The proposed system consists of FPC and HDH, and these systems are modeled using the following assumptions:

1. A steady-state condition is assumed.
2. The flow is incompressible.
3. Specific heat capacity, thermal conductivity and density of air and seawater are fixed.
4. Pressure drop is disregarded within the system.
5. As the system is working as a stationary component, kinetic and potential energy terms are neglected from the energy balance equations.
6. Heat loss from the HDH system to the surroundings is assumed to be zero, assuming the insulated components work 100% efficiently.
7. Air is saturated at the end of the dehumidifier and humidifier.

Flat-plate collector (FPC)

The Flat Plate Collector (FPC) converts solar radiation into thermal energy, which is absorbed by the fluid inside the FPC tubes. The fluid temperature increases linearly with higher solar intensity. In this case, the fluid is seawater. The glazing

NUST Journal of Engineering Sciences (NJES) is licensed under a Creative Commons Attribution 4.0 International License.

cover allows solar radiation to enter and be captured by the plate. Therefore, the overall heat loss coefficient of the FPC depends on the solar irradiation and convection heat losses to the surroundings. The top overall heat transfer coefficient, denoted by U_t on the top side of the FPC, was obtained as follows [13, 14].

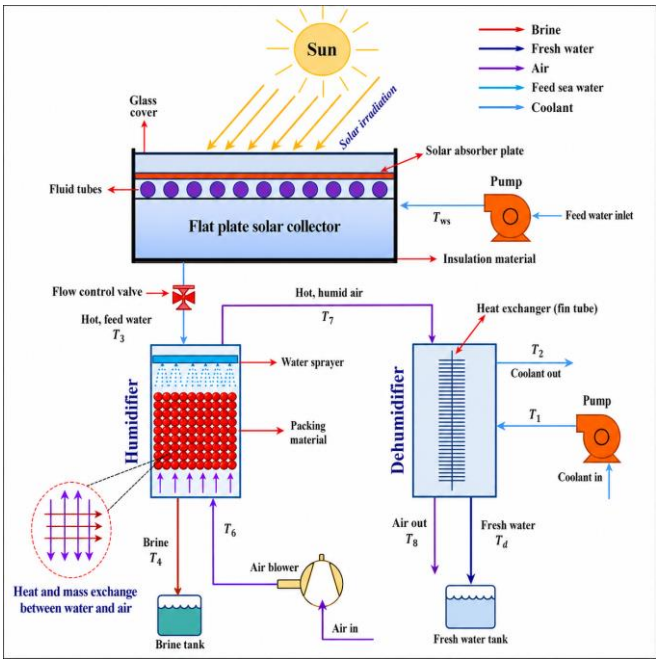

Figure 1: Schematic of Proposed FPC-driven HDH desalination system

Mathematical model of FPC

$$U_t = \left[\frac{N}{\frac{C}{Tpm}\left(\frac{T_{pm}-T_{amb}}{N+f}\right)e} + \frac{1}{h_{wind}}\right] - 1 + \frac{\sigma(T_{p.m} + T_{amb})(T2_{Pm} + T2_{amb})}{\frac{1}{\varepsilon p + 0.00591\, Nh_{wind}} + \frac{2N+f-1+0.133\varepsilon p}{\varepsilon p} - N} \quad (1)$$

where N is the number of glazings, T_{pm} shows the mean temperature of the absorber plate; T_{amb} is the ambient temperature; h_{wind} is the convective heat transfer coefficient on the outside of the FPC; σ is the Boltzmann constant, which is equal to 5.67×10^{-8} W/m^2.K^4, ε_g and ε_p represent the emittance of the glazing cover absorber fins, respectively. The coefficients f, C, and e are evaluated using equations (2) and (3) described under [13, 14] as follows:

$$f = (1 + 0.089_{hwind} - 0.1166_{hwind\varepsilon p})(1 + 0.07866N) \quad (2)$$

$$C = 520(1 - 0.000051\beta^2) \quad (3)$$

$$e = 0.43\left(1 - \frac{100}{Tp,m}\right) \quad (4)$$

where β is the collector slope. The bottom heat loss coefficient U_b was expressed as follows [14].

$$U_b = \frac{k_{ins}}{L_{ins}} \quad (5)$$

where K_{ins} is the thermal conductivity of insulation, and Lins is the length of insulation. The overall heat loss coefficient (U_{loss}) of the FPC is given as follows [14].

$$U_{loss} = U_t + U_b \quad (6)$$

The average fluid (T_{fm}) and absorber plate (T_{pm}) temperatures are calculated from the following equations.

$$T_{fm} = T_{fi} + \frac{\frac{qu}{A_{col}}}{F_R U_{loss}}(1 - F'') \quad (7)$$

$$T_{pm} = T_{fi} + \frac{\frac{qu}{A_{col}}}{F_R U_{loss}}(1 - F_R) \quad (8)$$

where T_{fi} is the seawater temperature at the outlet of the FPC, q_u denotes the useful heat gained by the tubes, A_{col} denotes the collector area, F_R denotes the FPC heat removal factor, and F" denotes the FPC flow factor. The outlet temperature (T_{fi}) of the seawater from the FPC was calculated as follows [13, 14].

$$\frac{T_{f0} - T_{amb} - \frac{S}{U_{loss}}}{T_{fi} - T_{amb} - \frac{S}{U_{loss}}} = \exp\left(-\frac{U_{loss}F'A_{col}}{\dot{m}_f c_{pw}}\right) \quad (9)$$

Here, T_{f0} denotes the inlet seawater temperature, S denotes the absorbed solar irradiation, F' denotes the FPC efficiency, c_{pw} denotes the specific heat coefficient, and $\dot{m}_f$ denotes the mass flow rate of the seawater. The variable F' was calculated as follows [14].

$$F' = \frac{\frac{1}{U_{loss}}}{W\left[\frac{1}{U_{loss}[D+(W-D)F]} + \frac{1}{h_f - i\pi D}\right]} \quad (10)$$

where W, D, F, and h_{fi} denote the width of the absorber Plate, outer diameter of the FPC tube, efficiency, and heat transfer coefficient, respectively. The FPC flow factor (F") denotes the ratio of the heat removal factor (FR) and FPC efficiency (F′), which can be determined as follows.

$$F'' = \frac{FR}{F'} = \frac{\dot{m}_f c_{pw}}{A_{col}U_{loss}F'}\left[1 - \exp\left(-\frac{A_{col}U_{loss}F'}{\dot{m}_f c_{pw}}\right)\right] \quad (11)$$

NUST Journal of Engineering Sciences (NJES) is licensed under a Creative Commons Attribution 4.0 International License.

The heat transfer coefficient, efficiency, absorbed solar irradiation, and useful heat gained by the tubes were calculated as follows [13, 14].

$$h_{fi} = \frac{k_{sw} Nu}{Di} \tag{12}$$

$$F = \frac{\tanh[m(W - D)/2]}{m(W - D)/2} \tag{13}$$

$$S = I_b R_b (\alpha\tau)_b + I_d (\alpha\tau)_v \left(\frac{1 + \cos\beta}{2}\right) + \rho_g I (\alpha\tau)_g \left(\frac{1 - \cos\beta}{2}\right) \tag{14}$$

$$qu = A_{col} FR [S - U_{loss}(T_{f-i} - T_{amb})] \tag{15}$$

where k_{sw} denotes the thermal conductivity of the seawater, Nu denotes the Nusselt number, D_i denotes the internal diameter of the absorption tube, R_b denotes the ratio of beam radiation on a tilted plane (θ) and the plane of measurement (θz), ατ denotes the absorptance-transmittance product, I denotes the solar irradiation, and FR denotes the heat removal factor. The Nusselt numbers for laminar and turbulent flows are evaluated as follows [14].

$$Nu = 3.66 \quad Re < 2300 \tag{16}$$

$$Nu = 0.023 Re^{0.8} Pr^{0.4} \quad Re > 10000 \tag{17}$$

where Re denotes the Reynolds number, and Pr denotes the Prandtl number. The Nusselt number for Re in the range of 2300 to 10000 was determined using linear interpolation. The variables Re, m, and Rb are determined as follows.

$$Re = \frac{D_i V_f \rho_f}{\mu_f} \tag{18}$$

$$m = \sqrt{\frac{U_{loss}}{k\delta}} \tag{19}$$

$$R_b = \frac{\cos\theta}{\cos\theta_z} \tag{20}$$

where V_f denotes the velocity of the feedwater, ρf denotes the density of the feed, μf denotes the viscosity of the feed, k denotes the thermal conductivity of the heat-absorbing tube, and δ denotes the thickness of the absorber fin. The collector heat removal factor (FR) is the amount of actual useful energy gained by the flat plate collector from the actual useful energy, and it was determined as follows:

$$FR = \frac{\dot{m}_f c_{pw}(T_{f0} - T_{fi})}{A_{col}[S - U_{loss}(T_{fi} - Tamb)]} = \frac{\dot{m}_f c_{pw}}{A_{col} U_{loss}} \left[1 - \exp\left(-\frac{A_{col} U_{loss} F'}{\dot{m}_f c_{pw}}\right)\right] \tag{21}$$

The hourly climatic data for Gwadar were obtained from RETScreen and organized in Microsoft Excel in xlsx format. They were then imported from the Excel file into MATLAB using the readtable() function. These data were then used as input parameters in the numerical model to solve the governing equations for the flat plate collector and HDH system. The calculated outlet conditions were transferred sequentially between the system components.

Mathematical model of HDH system

The mass and energy balance equations of humidification–dehumidification processes are presented in this section. Under steady-state and no-heat-loss conditions, the energy balance during the humidification process is described as [15].

The energy balance is equal to:

$$Q_{in} - Q_{out} - Q_{loss} = 0 \tag{22}$$

Since there are no heat-loss conditions Q_{loss} will be canceled.

Then the energy balance would be:

$$Q_{in} - Q_{out} = 0 \tag{23}$$

Humidifier energy balance

Energy entering and leaving the humidifier is expressed as follows:

$$\dot{m}_w H_{w3} + \dot{m}_{air} H_{a6} = \dot{m}_b H_{w4} + \dot{m}_{air} \dot{m}_{a7} \tag{24}$$

where H_{w3} and H_{w4} are the enthalpies of seawater at the inlet and outlet of the humidifier unit, respectively. Further, H_{a6} and H_{a7} are the enthalpies of air at the humidifier inlet and exit, respectively; and $\dot{m}_w$, $\dot{m}_{air}$ and $\dot{m}_b$ denote the mass flow rates of water, air, and brine, respectively. The mass balance in the humidifier unit is expressed as:

Mass balance inside the humidifier

The mass balance inside the humidifier is represented as follows:

$$\dot{m}_b = \dot{m}_w - \dot{m}_{air}(\omega_7 - \omega_6) \tag{25}$$

where ω_7 is the humidity ratio at the humidifier outlet, and ω_6 is the humidity ratio at the humidifier inlet. Another equation is needed to complete the solution; Hence,

Effectiveness of the humidifier

The effectiveness of the humidifier is introduced as under [15].

$$\varepsilon h = \max\left[\frac{H_{a7} - H_{a6}}{H_{a7,ideal} - H_{a6}}, \frac{H_{w3} - H_{w4}}{H_{w3} - H_{w4,ideal}}\right] \tag{26}$$

NUST Journal of Engineering Sciences (NJES) is licensed under a Creative Commons Attribution 4.0 International License.

where $H_{a7,ideal}$ is the ideal enthalpy of air at the humidifier outlet calculated by setting the air temperature equal to the inlet temperature of seawater, and $H_{w4,ideal}$ is the ideal enthalpy of seawater at the humidifier outlet calculated by setting the seawater temperature equal to the air temperature at the humidifier inlet.

Dehumidifier energy balance

The energy balance across the dehumidifier is given by [16].

$$\dot{m}_{cw}\, c_w\, T_1 + \dot{m}_{air} H_{a7} = \dot{m}_{cw} c_w\, T_2 + \dot{m}_d H_d + \dot{m}_{air} H_{a8} \quad (27)$$

where $\dot{m}_{cw}$ is the coolant mass flow rate; T_1 and T_2 are the temperatures of cooling water at the dehumidifier inlet and outlet, respectively; $\dot{m}_d$ denotes the mass flow rate of distillate; and H_{a8} is the air enthalpy at the dehumidifier exit, and H_d is the enthalpy of distillate at a temperature T_d ", which is taken as the average of the inlet and outlet air temperatures inside the dehumidifier. The salt concentration in pure water is assumed to be less than 500 ppm, which is safe for consumption [17]. Similarly, the mass balance across the dehumidifier unit is expressed as:

Mass balance inside the dehumidifier

Mass balance of the dehumidification column is expressed as:

$$\dot{m}_d = \dot{m}_{air}(\omega_7 - \omega_8) \quad (28)$$

One more equation is needed to complete the solution; hence, the dehumidifier effectiveness is introduced as follows.

Effectiveness of the dehumidifier

$$\varepsilon d = \max\left[\frac{H_{a7} - H_{a8}}{H_{a7} - H_{a8,ideal}}, \quad \frac{H_{w2} - H_{w1}}{H_{w2,ideal} - H_{w1}}\right] \quad (29)$$

where $H_{a8,ideal}$ is the ideal enthalpy of air at the dehumidifier outlet calculated by putting the cooling water inlet temperature, and $H_{w2,ideal}$ is the ideal enthalpy of cooling water at the dehumidifier outlet, calculated by using the inlet air temperature [16] . H_{w1} and H_{w2} are the enthalpies of the inlet and outlet cooling water across the dehumidifier unit, respectively.

Other physical properties

The enthalpy of seawater is provided by [18] as under:

$$H_w = H_{pw} - s\begin{pmatrix} a_1 + a_2 s + a_3 s^2 + a_4 s^3 \\ + a_5 T + a_6 T^2 + a_7 T^3 \\ + a_8 s T + a_9 s^2 T + a_{10} s T^2 \end{pmatrix} \quad (30)$$

where H_{pw} is the enthalpy of pure water, and s is the seawater salinity level. The coefficients used above are listed in Table 2.

Table 2: Coefficients considered for seawater enthalpy calculation. [18].

a_1	-2.348×10^4	a_6	-44.17
a_2	3.15×10^5	a_7	2.139×10^{-1}
a_3	2.803×10^6	a_8	-1.997×10^4
a_4	-1.446×10^7	a_9	2.778×10^4
a_5	7.826×10^3	a_{10}	97.28

The enthalpy of pure water is given by [18].

$$Hpw = 141.355 + 4202.07\, T - 0.535\, T^2 + 0.004\, T^3 \quad (31)$$

The enthalpy of humid air is computed by [19].

$$H_a = (c_{air} + c_v \omega) T + h_{fg} \omega \quad (32)$$

where c_v is the heat capacity of vapor. The absolute humidity, ω, which is a function of relative humidity and dry air temperature, is expressed by the following [20].

$$\omega = 0.62198 \times \left[\frac{\varphi P_s}{P_{atm} - \varphi P_s}\right] \quad (33)$$

where φ is the relative humidity, and P_{atm} is the atmospheric pressure. The saturation pressure, P_s , is calculated by:

$$Ps = (2.7 \times 10^{-9} \times T^5) + (2.8 \times 10^{-7} \times T^4) + (2.7 \times T^{-5} \times T^3) + (0.0014 \times T^2) + (0.044 \times T) + 0.61 \quad (34)$$

In Equation (9), h_{fg} is the latent heat of water evaporation, which is expressed in a correlation that is valid over the temperature range 5–200 ◦C; it is given by [21].

$$h_{fg} = 2501.897149 - 2.407064037\, T + 1.192217 \times 10^{-3} \times T^2 - 1.5863 \times 10^{-5} \times T^3 \quad (35)$$

The performance of the HDH system is usually expressed with respect to the GOR, defined as [22].

$$GOR = \frac{\dot{m}_d h_{fg}}{S\, A_{col}} \quad (36)$$

where S denotes radiation, and A_{col} is the collector area, which is fixed at 1.5 m^2 [23] .

Boundary Conditions and Solution Method

The boundary conditions for the proposed system were established based on the system configuration shown in Figure 1 and the operating conditions considered in the parametric analysis. The FPC inlet temperature was specified

NUST Journal of Engineering Sciences (NJES) is licensed under a Creative Commons Attribution 4.0 International License.

using the seawater inlet temperature. In contrast, the collector outlet temperature was calculated from the solar collector model and used as the humidifier inlet water temperature T_3. The incident solar irradiance and ambient temperature were prescribed using the representative hourly climatic conditions for Gwadar, Pakistan, obtained from the RETScreen software. For the representative summer day, solar irradiance reached approximately 960 W/m², ambient temperature reached 39.2°C, and seawater inlet temperature varied from approximately 28.6°C to 34.1°C. The collector area was fixed at 1.5 m², as specified in the mathematical model.

At the humidifier inlet, the hot seawater supplied by the FPC and ambient air were treated as the incoming streams. The inlet air humidity ratio was determined from the inlet air temperature, relative humidity, and atmospheric pressure using the psychrometric relationships presented in Section 3.2. The humidifier outlet conditions were determined using the humidifier mass and energy balances and the specified humidifier effectiveness. The resulting humid-air state was subsequently used as the inlet condition for the dehumidifier. On the cooling side, the coolant inlet temperature T_1 and cooling-water mass flow rate were prescribed. In contrast, the coolant outlet temperature T_2, dehumidifier outlet air condition, and freshwater production rate were determined from the dehumidifier model and its effectiveness relationship. The simulations were performed under the assumptions specified in Section 3. The operating parameters were varied individually or in combination within the ranges specified in the parametric analyses, while the remaining boundary conditions were held constant for each comparison. The calculated outlet state of each component was passed to the next component to maintain consistency between the FPC, humidifier, and dehumidifier models. Equations (22)– (29) were solved using the fsolve function in MATLAB R2025b. After solving these equations, productivity and GOR were calculated. Equations (30)–(35) are supplementary equations for determining the enthalpies of seawater and humid air. The MATLAB solver convergence was controlled by setting the function and step tolerances to 10^{-8}, and convergence was accepted when the residuals met the specified tolerance and the calculated mass and energy balances were physically consistent.

Economic Analysis of the Proposed System

The economic feasibility of the proposed solar-driven humidification–dehumidification (HDH) desalination system was evaluated using the levelized cost of water (LCOW). LCOW represents the average cost to produce one liter of freshwater over the system's full operating life. This method suits small-scale solar desalination systems because it accounts for initial capital cost, annualized investment, operation and maintenance cost, expected system lifetime, and annual freshwater production. In this study, the LCOW was used to assess whether the proposed flat plate collector-assisted HDH system is a practical option for decentralized freshwater production in Gwadar.

Capital Cost Estimation

The total capital cost of the proposed system includes the major components required for fabrication and operation, such as the flat plate solar collector, humidifier, dehumidifier, pump, blower, piping, storage tank, support structure, and packing material. The cost values were estimated based on small-scale fabrication and local market conditions in Pakistan. The component-wise cost breakdown is presented in Table 3**.**

Table 3: Estimated capital cost of the proposed solar-driven HDH desalination system.

Component	**Estimated cost (PKR)**
Flat plate solar collector, 1.5 m²	35,000
Humidifier with packing material	15,000
Dehumidifier/condensing unit	10,000
Pump, blower, and piping system	10,000
Storage tank and support structure	10,000
Total capital cost (C_0)	**80,000**

Annualized Capital Cost

The initial capital investment was converted into an equivalent annual cost using the capital recovery factor (CRF). This approach spreads the capital investment over the system's useful life. The annualized capital cost is expressed as:

$$C_{ann} = C_0 \times CRF \tag{37}$$

where C_{ann} is the annualized capital cost, and C_0 is the total capital cost of the system. The capital recovery factor is calculated as:

$$CRF = \frac{i(1+i)^n}{(1+i)^n - 1} \tag{38}$$

where i is the annual interest or discount rate, and n is the expected lifetime of the system. In this analysis, the discount rate and system lifetime were assumed to be 10% and 15 years, respectively. The economic assessment was conducted using a reference plant lifetime of 15 years and an annual discount rate of 10%. The total initial capital cost of the proposed FPC–HDH desalination system was estimated at PKR 80,000, based on the component-wise cost breakdown presented in Table 3. The initial investment was converted into an equivalent annual capital cost using the capital recovery factor (CRF), resulting in an annualized capital cost of approximately PKR 10,480/year. The annual operation and maintenance (O&M) cost was estimated as 5% of the initial capital cost, corresponding to PKR 4,000/year. Accordingly, the total base-case annualized cost was PKR 14,480/year, excluding auxiliary electricity costs and any separately estimated component replacement expenditure. These

NUST Journal of Engineering Sciences (NJES) is licensed under a Creative Commons Attribution 4.0 International License.

assumptions provide the reference basis for the LCOW calculations presented in this study.

Operation and Maintenance Cost

The annual operation and maintenance cost includes periodic cleaning of the solar collector, inspection of the humidifier packing material, removal of salt deposition, pump and blower servicing, replacement of minor fittings, leakage control, and general maintenance. Because the system is mainly driven by solar thermal energy, regular operating costs are relatively low. The annual operation and maintenance cost was estimated as a fixed percentage of the initial capital cost:

$$C_{O\&M} = f_{O\&M} \times C_0 \tag{39}$$

where $C_{O\&M}$ is the annual operation and maintenance cost, while $f_{O\&M}$ is the maintenance cost factor, which was assumed to be 5% of the total capital cost. Therefore, $C_{O\&M}$ = 0.05×80000 = 4000 PKR/year.

The total annual cost of the system is then calculated as:

$$C_{total,ann} = C_{ann} + C_{O\&M} + C_{el} \tag{40}$$

where C_{el} is the annual auxiliary electricity cost for the pump and blower. In the present analysis, the auxiliary electricity cost was considered small compared with the capital and maintenance costs. Therefore, for the base economic case, C_{el} was neglected. Hence, $C_{total,\,ann}$ = 14480 PKR/year.

The economic assessment assumes that the major system components remain operational throughout the reference plant lifetime of 15 years. Separate costs for replacing the solar collector, humidifier packing, pumps, blower, dehumidifier components, or other equipment were not included because component-specific service-life data and replacement-cost estimates were unavailable. Similarly, salvage value and decommissioning costs were excluded from the analysis. Therefore, the reported LCOW represents an estimate based on the specified initial capital investment and annual O&M allowance rather than a complete life-cycle cost assessment. Excluding component replacement expenditure may underestimate the long-term cost of freshwater production if any components require replacement during the plant lifetime. This limitation should be considered when interpreting the economic results.

Annual Freshwater Production

The annual freshwater production was estimated from the distillate production rate obtained from the thermodynamic model. The freshwater production rate varies with solar radiation, ambient temperature, seawater inlet temperature, humidifier inlet temperature, and air mass flow rate. Therefore, the maximum hourly productivity should not be directly used as the annual average value. Instead, the annual production should be calculated using the daily effective operating duration and the number of operating days. The annual freshwater production can be expressed as:

$$M_{ann} = N_{op} \sum_{i=1}^{N_h} \dot{m}_{d,t} \Delta t \tag{41}$$

where M_{ann} is the annual freshwater production in L/year, N_{op} is the number of operating days per year, N_h is the number of effective sunshine hours per day, $\dot{m}_{d,t}$ is the hourly distillate production rate in kg/h, and Δt is the time interval. Since the density of freshwater is approximately 1 kg/L, freshwater production in kg is approximately equal to freshwater production in liters. For monthly analysis, the annual freshwater production may also be calculated as:

$$M_{ann} = \sum_{j=1}^{12} N_j \dot{m}_{d,j} \tag{42}$$

where N_j is the number of operating days in the jth month and $M_{d,j}$ is the average daily freshwater production in that month.

Levelized Cost of Water

The levelized cost of water was calculated by dividing the total annual cost by the annual freshwater production:

$$LCOW = \frac{C_{ann} + C_{O\&M} + C_{el}}{M_{ann}} \tag{43}$$

where LCOW is expressed in PKR/L. This equation shows that water production cost depends strongly on annual freshwater yield. Therefore, a single LCOW value may not represent the entire system behavior unless the annual production basis is clearly defined. To avoid overestimating the economic performance, different annual freshwater production scenarios were considered. The resulting LCOW values are shown in Table 4.

Table 4: LCOW sensitivity to annual freshwater production.

Average freshwater production	Annual freshwater production	Estimated LCOW
2.2 L/day	804 L/year	18.0 PKR/L
5 L/day	1825 L/year	7.9 PKR/L
10 L/day	3650 L/year	4.0 PKR/L
20 L/day	7300 L/year	2.0 PKR/L
36 L/day	10800 L/year	1.34 PKR/L

The results show that an LCOW of approximately 18 PKR/L corresponds to a highly conservative production case of nearly 2.2 L/day. However, when the system operates for longer effective sunshine hours and produces higher daily freshwater yield, the LCOW decreases significantly. For example, if the system produces about 10 L/day, the LCOW decreases to approximately 4 PKR/L. Therefore, the economic performance of the proposed system is highly sensitive to the actual daily productivity and annual operating period. The economic results indicate that the proposed solar-

NUST Journal of Engineering Sciences (NJES) is licensed under a Creative Commons Attribution 4.0 International License.

driven HDH desalination system can be feasible for small-scale freshwater production in Gwadar, particularly under favorable solar radiation and thermal conditions. However, the LCOW should be interpreted as a production-dependent value rather than a fixed cost. Therefore, instead of reporting a single water cost value, this study reports a cost range based on different annual freshwater production scenarios. This provides a more realistic and transparent economic assessment of the proposed system.

Results and Discussion

To establish the climatic boundary conditions for the FPC–HDH simulation, the hourly variation of solar irradiance, ambient temperature, and seawater inlet temperature for a representative hot summer day in June at Gwadar is presented in Figure 2. Solar irradiance increased sharply after sunrise and peaked at approximately 960 W/m² around 1:00 PM, indicating strong midday solar availability for the flat plate collector. During the same period, the ambient temperature increased from 31.2°C in the morning to nearly 39.2°C in the afternoon, while the seawater inlet temperature increased more gradually from 28.6°C to 34.1°C because seawater has higher thermal inertia. The simultaneous increase in solar irradiance and feedwater temperature reduces the thermal load required from the collector and supports higher humidifier inlet temperatures. Therefore, the period between 12:00 PM and 3:00 PM is expected to provide the most favorable operating window for evaporation, freshwater productivity, and GOR.

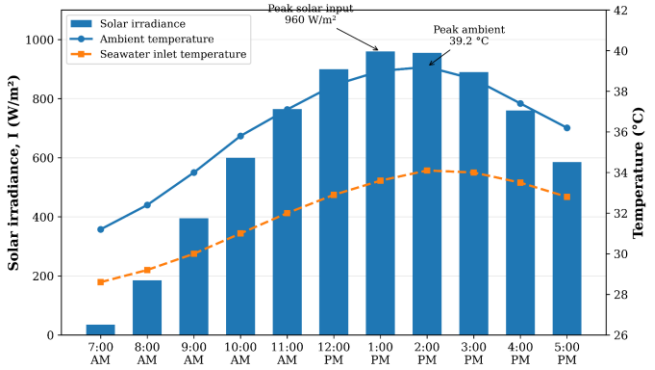

Figure 2: Hourly climatic boundary conditions for Gwadar on a representative hot summer day in June (RETScreen)

The thermal response of the flat plate collector under the climatic boundary conditions of June is presented in Figure 3. The FPC outlet temperature, which also represents the humidifier inlet water temperature T_3, increased from 31.0°C in the morning to a maximum of 90.1°C around 1:00 PM. This trend follows the increase in solar irradiance and useful heat gain during the same period. Useful heat gain increased from 0.028 kW at 7:00 AM to a peak of approximately 0.66 kW at 1:00 PM, then gradually decreased as solar input declined in the afternoon. The seawater inlet temperature increased more slowly than the outlet temperature because of seawater's thermal inertia; however, its gradual rise from 28.6°C to above 34°C reduced the temperature lift required inside the collector. The modeled midday collector efficiency remained within approximately 43.6–46.7%, indicating that a significant portion of the incident solar energy was converted into useful thermal energy.

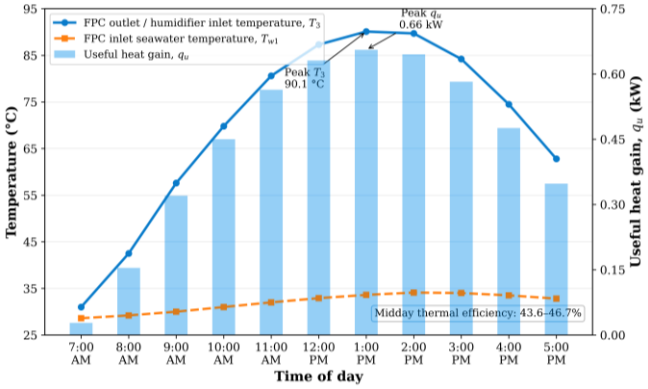

Figure 3: Hourly thermal response of the flat plate collector under Gwadar hot summer-day conditions.

Parametric performance of the flat plate collector

To further evaluate the thermal behavior of the flat plate collector, the combined effect of solar irradiance and seawater mass flow rate on the FPC outlet temperature is presented in Figure 4. The outlet temperature increased with increasing solar irradiance because higher incident radiation increased the absorbed solar energy and the collector's useful heat gain. In contrast, increasing the seawater mass flow rate reduced the outlet temperature because the absorbed heat was distributed over a larger water flow rate, decreasing the temperature rise across the collector.

At low feedwater flow rates below approximately 0.004 kg/s, the collector produced outlet temperatures above 80°C when solar irradiance exceeded 850 W/m². This region is particularly favorable for HDH desalination because high humidifier inlet water temperature increases the vapor pressure difference between hot saline water and air, thereby improving moisture transfer inside the humidifier. The representative June peak operating point, corresponding to solar irradiance of approximately 960 W/m² and seawater mass flow rate of 0.0029 kg/s, produced an FPC outlet temperature close to 90°C. This agrees with the hourly thermal response discussed earlier and confirms that the selected low-flow operating condition is suitable for achieving high-temperature feedwater for the HDH cycle. However, the contour also shows that increasing the seawater flow rate above 0.008–0.010 kg/s significantly lowers the outlet temperature, even under strong solar radiation. This indicates that the seawater flow rate should not be increased only to raise water throughput, because excessive flow weakens the thermal quality of the feedwater entering the humidifier. Therefore, an optimum operating range exists where the collector provides sufficient thermal energy while maintaining a practical water flow rate for humidification.

NUST Journal of Engineering Sciences (NJES) is licensed under a Creative Commons Attribution 4.0 International License.

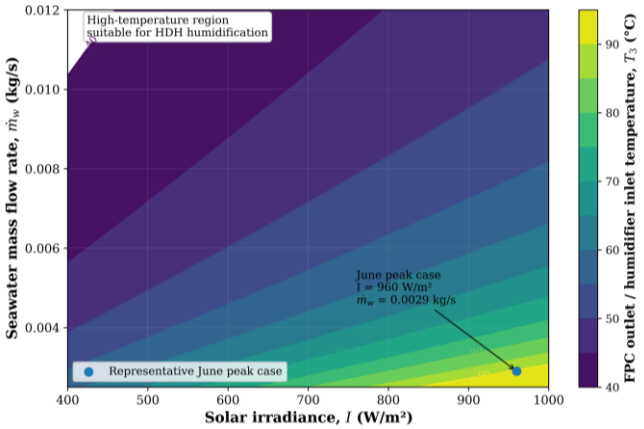

Figure 4: Effect of solar irradiance and seawater mass flow rate on the FPC outlet/humidifier inlet temperature under hot summer conditions in Gwadar.

Effect of absorber material on FPC thermal output

The absorber plate material is a critical design parameter for the flat plate collector because it controls how effectively the absorbed solar radiation is transferred from the heated absorber surface to the seawater flowing through the tubes. The effect of absorber material on the FPC outlet temperature is illustrated in Figure 5. Under the same climatic boundary conditions, collector area, seawater inlet temperature, and mass flow rate, the copper absorber produced the highest outlet temperature throughout most of the operating period. The maximum outlet temperature reached approximately 90.1°C for copper, followed by 87.6°C for aluminum and 80.2°C for steel. This difference is mainly due to copper's higher thermal conductivity, which reduces conduction resistance between the absorber plate and the tube wall and improves the collector surface's heat-spreading ability.

During the morning period, the differences among the three absorber materials were relatively small because incident solar radiation was still low and available thermal energy was limited. As solar irradiance increased toward midday, the material effect became more pronounced. This behavior indicates that absorber material selection becomes more important under high-radiation conditions, when the absorber plate temperature increases and more heat must be transferred to the working fluid. The copper absorber maintained the strongest thermal response because its high conductivity allowed rapid heat transfer from the absorber plate to the seawater, leading to higher useful heat gain and higher humidifier inlet temperature.

The aluminum absorber showed performance close to copper, especially during peak solar hours. The maximum temperature difference between copper and aluminum remained modest, suggesting that aluminum may be a practical alternative when cost, weight, and corrosion protection are important design considerations. However, even a small reduction in humidifier inlet temperature can affect HDH performance because water vapor pressure increases nonlinearly with temperature. Therefore, the slightly lower outlet temperature with aluminum may still reduce the air's moisture-carrying capacity and final freshwater production compared with copper.

The steel absorber produced the lowest outlet temperature over the entire day. At peak solar conditions, the steel-based collector reached only about 80.2°C, which is nearly 10°C lower than the copper case. This reduction is significant for HDH desalination because the humidification process is strongly driven by the temperature difference between hot saline water and air. Lower feedwater temperature reduces water vapor pressure, decreases evaporation intensity, and weakens the enthalpy rise of the humid air leaving the humidifier. Consequently, although steel is mechanically strong and relatively inexpensive, its lower thermal conductivity makes it less suitable as the primary absorber material for a solar HDH system where high water temperature is required. The 70°C reference line in Figure 5 represents a practical threshold above which strong humidification can be expected. Copper and aluminum maintained temperatures above this level longer during the day, particularly from about 11:00 AM to 4:00 PM. In contrast, steel remained near or below this threshold for a larger portion of the operating window. This means a steel absorber would shorten the HDH unit's effective high-productivity period and reduce daily freshwater yield. The peak useful heat gain was approximately 0.66 kW for copper, 0.63 kW for aluminum, and 0.54 kW for steel, confirming that steel's inferior thermal behavior directly reduces the thermal energy delivered to the humidifier.

Overall, the results indicate that copper is the most suitable absorber material for maximizing thermal output and freshwater productivity in the proposed FPC–HDH desalination system. Aluminum can serve as a cost-effective alternative with a moderate reduction in thermal performance. Meanwhile, steel is not recommended when the design objective is to achieve a high humidifier inlet temperature. Therefore, for Gwadar's hot, high-radiation summer conditions, strong solar input and a high-conductivity absorber material are essential to sustain high evaporation rates and improve the overall performance of the HDH cycle.

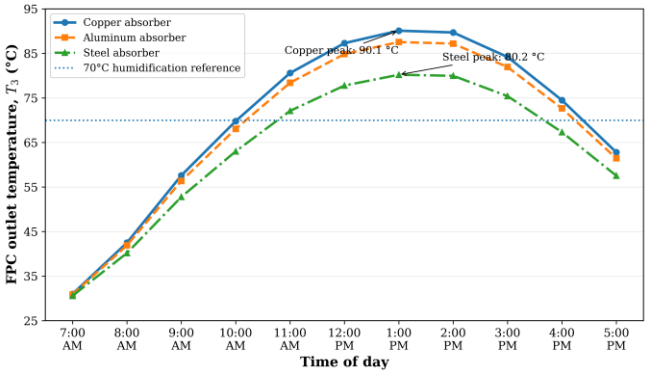

Figure 5: Effect of absorber material on the FPC outlet/humidifier inlet temperature under Gwadar hot summer-day operating conditions.

NUST Journal of Engineering Sciences (NJES) is licensed under a Creative Commons Attribution 4.0 International License.

Effect of insulation material on FPC thermal output

The influence of insulation material on the FPC outlet temperature is presented in Figure 6. In the flat plate collector model, insulation affects the bottom heat-loss coefficient, which is calculated from the ratio of insulation thermal conductivity to insulation thickness. Therefore, lower thermal conductivity reduces bottom-side heat leakage and improves the useful heat retained by the collector. Under the same collector area, absorber material, seawater mass flow rate, and climatic boundary conditions, polyurethane insulation produced slightly higher outlet temperatures than mineral wool.

The maximum outlet temperature reached approximately 90.1°C for polyurethane, whereas mineral wool produced a peak value of about 88.1°C. Although the difference is smaller than the effect of absorber material, it is still important because the HDH cycle is highly sensitive to the humidifier inlet temperature. The bottom heat-loss coefficient was approximately 0.50 W/m²K for polyurethane and 0.90 W/m²K for mineral wool under the considered insulation thickness. This higher heat-loss coefficient increased thermal leakage from the collector casing and slightly reduced the useful heat delivered to the seawater. The temperature penalty caused by mineral wool became more visible during the high-radiation period, especially between 11:00 AM and 3:00 PM. This occurs because the absorber plate and fluid temperatures are highest during midday, increasing the temperature difference between the collector and surroundings. A larger temperature difference increases heat loss through the bottom and side surfaces, making insulation more important during peak operation. Consequently, the peak useful heat gain decreased from approximately 0.66 kW with polyurethane to 0.63 kW with mineral wool. Both insulation materials allowed the collector to maintain temperatures above the 70°C humidification reference for several hours. However, polyurethane sustained a slightly wider high-temperature operating window and therefore provides better conditions for moisture generation in the humidifier. Because higher feedwater temperature increases vapor pressure and improves heat and mass transfer between saline water and air, even a small improvement in FPC outlet temperature can improve freshwater productivity and GOR. Overall, polyurethane is preferred for the proposed FPC–HDH system because it reduces collector heat loss more effectively and improves thermal energy delivery to the humidifier.

Humidifier performance under variable feedwater temperature and air flow rate

To examine the transition from the solar collector subsystem to the HDH unit, the combined effect of humidifier inlet water temperature and air mass flow rate on the outlet humid-air condition is presented in Figure 7. The humidifier inlet water temperature (T3) represents the hot feedwater temperature supplied by the flat plate collector. Therefore, improvements in collector thermal output directly affect the heat and mass transfer process inside the humidifier. The outlet humidity ratio increased strongly with increasing T3. This behavior is physically expected because higher feedwater temperature increases the saturation vapor pressure at the water–air interface, which strengthens the vapor pressure gradient between the hot saline water and the flowing air stream. As a result, more water vapor is transferred from the liquid phase to the air phase. When (T_3) increased from 55°C to 90°C, the humidifier outlet humidity ratio increased substantially, especially in the low-to-moderate air flow region. This confirms that FPC outlet temperature is one of the most important parameters controlling the air's moisture-carrying capacity.

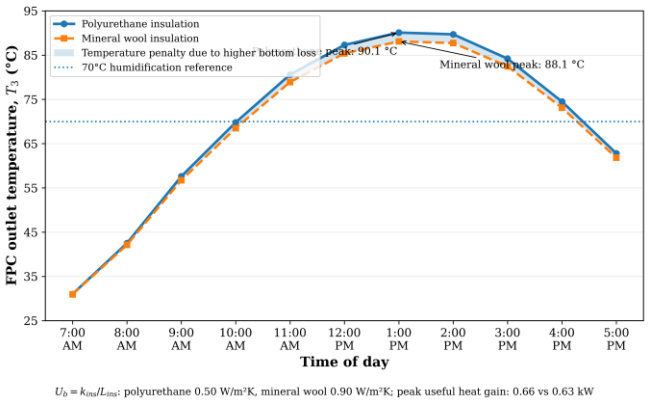

Figure 6: Effect of insulation material on the FPC outlet/humidifier inlet temperature under Gwadar hot summer-day operating conditions.

Air mass flow rate had the opposite effect on the humidity ratio per unit mass of dry air. At lower air flow rates, the air had a longer contact time with the hot water and approached a higher outlet temperature. Therefore, the air leaving the humidifier carried more moisture. However, when the air mass flow rate increased, the same thermal energy was distributed over a larger air stream, reducing the outlet air temperature and the humidity ratio per kilogram of dry air. This explains why the contour bands shift toward lower humidity ratio at higher air mass flow rates.

The overlaid (T_7) contours further clarify the humidifier's thermal behavior. At higher (T_3) and lower air flow rates, the humidifier outlet air temperature approached nearly 70–72°C, indicating strong heat transfer from hot feedwater to air. For the marked high-temperature operating condition of ($T_3 \sim 90$ °C and $\dot{m}_a = 0.025$ kg/s), the outlet air temperature reached approximately 71.7°C, while the outlet humidity ratio reached about 0.309 kg/kg dry air. These values indicate a highly humid air stream entering the dehumidifier, which favors subsequent condensation and freshwater recovery. Although a lower air mass flow rate increases the humidity ratio, it does not automatically guarantee the highest freshwater production because the total vapor transport also depends on the amount of dry air circulated through the system. Therefore, an optimum air flow rate is expected, where the reduction in humidity ratio at higher air flow is balanced by the larger air throughput. This interaction between humidity ratio and air

NUST Journal of Engineering Sciences (NJES) is licensed under a Creative Commons Attribution 4.0 International License.

flow rate is important for optimizing the HDH cycle and will directly influence the freshwater productivity and GOR in the following analysis.

Effect of air mass flow rate and humidifier inlet temperature on freshwater productivity

The influence of air mass flow rate on freshwater productivity at different humidifier inlet water temperatures is presented in Figure 8. The humidifier inlet water temperature (T3) represents the thermal output supplied by the flat plate collector to the HDH unit. Therefore, this figure directly links solar collector performance to the desalination system's freshwater production capacity. Freshwater productivity increased with increasing (T_3) because higher feedwater temperature enhanced the evaporation potential inside the humidifier. At higher (T_3), the vapor pressure at the hot-water surface increased significantly, strengthening the vapor-pressure gradient between the water stream and the air stream.

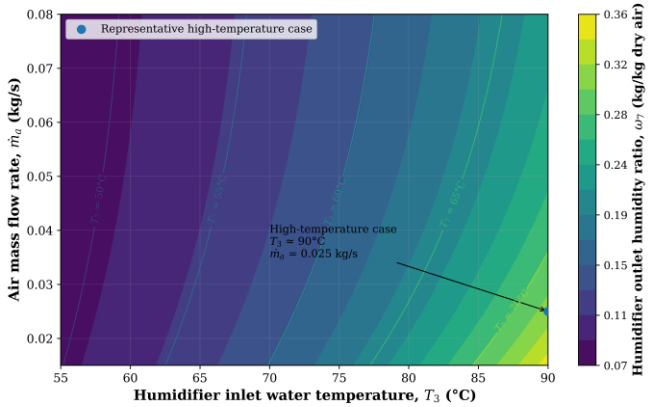

Figure 7: Effect of humidifier inlet water temperature and air mass flow rate on the humidifier outlet humidity ratio under hot summer operating conditions in Gwadar at T_7 = 71.7 °C and ω_7 = 0.0309 kg/kg dry air.

This allowed the air to absorb more moisture before entering the dehumidifier. Consequently, at a fixed air mass flow rate, the freshwater production increased strongly as (T_3) increased from 60°C to 90°C. At (T_3 = 60 °C), the productivity remained relatively low, increasing from approximately 0.46 kg/h to 1.14 kg/h as the air mass flow rate increased from 0.015 kg/s to 0.080 kg/s. This is because the thermal driving force for evaporation was limited at lower feedwater temperatures. When (T_3) increased to 70°C and 80°C, the maximum productivity improved to approximately 2.34 kg/h and 3.99 kg/h, respectively. The most favorable performance was obtained at (T_3 = 90 °C), where productivity increased from about 2.53 kg/h at low air flow rate to nearly 6.34 kg/h at the highest considered air flow rate. The increase in productivity with air mass flow rate is associated with the larger amount of dry air passing through the humidifier. Although the humidity ratio per unit mass of dry air may decrease at higher air flow rates because of shorter contact time, the total mass of air available for carrying water vapor increases. Therefore, the total vapor transport to the dehumidifier increases with air mass flow rate within the investigated range. This explains why productivity continues to increase as air mass flow rate rises, particularly at higher T_3 values. However, the slope of the productivity curve gradually decreases at higher air mass flow rates. This indicates that the benefit of increasing air flow weakens when the contact time between air and hot water decreases. At very high air flow rates, the air may leave the humidifier before approaching thermal and humidity equilibrium with the hot water. Therefore, further increases in air flow would require a larger humidifier or improved packing design to maintain effective heat and mass transfer. Overall, the results confirm that high humidifier inlet water temperature and sufficient air circulation are both necessary for improving freshwater production. The favorable case of (T_3 = 90 °C and $\dot{m}_a$ = 0.080 kg/s) produced approximately 6.34 kg/h of freshwater, which supports the suitability of the proposed FPC–HDH system for small-scale freshwater production during high-radiation summer conditions in Gwadar.

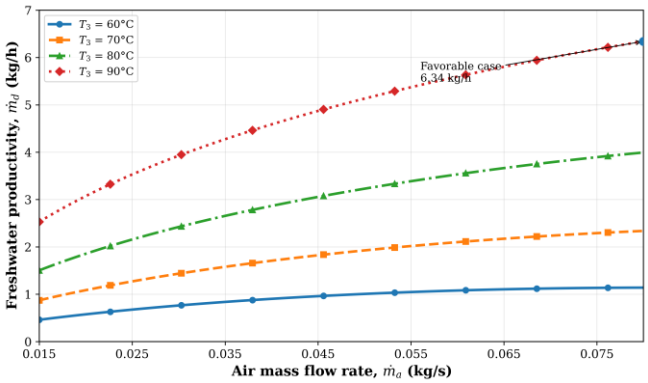

Figure 8: Effect of air mass flow rate on freshwater productivity at different humidifier inlet water temperatures.

Effect of air mass flow rate and humidifier inlet temperature on GOR

The effect of air mass flow rate on the gain output ratio at different humidifier inlet water temperatures is presented in Figure 9. Unlike freshwater productivity, which mainly represents the amount of condensed water, GOR evaluates how effectively the supplied thermal energy is converted into latent heat recovery through freshwater production. Therefore, GOR is a more useful indicator for assessing the thermal efficiency of the HDH cycle.

The GOR increased significantly with increasing humidifier inlet water temperature. At (T_3 = 60 °C), the GOR remained below 0.8 over the entire airflow range because the vapor pressure difference between hot water and air was relatively weak. As T_3 increased to 70°C and 80°C, the GOR improved to approximately 1.39 and 2.05, respectively. This improvement occurs because higher feedwater temperature increases the humidity ratio of the air leaving the humidifier, thereby increasing the amount of vapor available for condensation in the dehumidifier. The highest GOR was obtained at (T_3 = 90 °C), where the value increased from approximately 1.96 at low air flow rate to a maximum of

NUST Journal of Engineering Sciences (NJES) is licensed under a Creative Commons Attribution 4.0 International License.

about 2.62 at an air mass flow rate of nearly 0.061 kg/s. This confirms that a high humidifier inlet temperature is essential for improving the thermal performance of the HDH system. Under this condition, the airstream carries a large amount of water vapor, and the dehumidifier can recover a higher fraction of latent heat as freshwater. However, the GOR did not increase indefinitely with air mass flow rate. At low-to-moderate air flow rates, increasing ($\dot{m}_a$) improved vapor transport from the humidifier to the dehumidifier, which increased both productivity and GOR. Beyond the optimum region, the improvement weakened, and the GOR slightly decreased in the highest-temperature case. This behavior is physically reasonable because excessive airflow reduces the air residence time inside the humidifier and increases the airstream's sensible heating demand. As a result, additional thermal energy is consumed in heating a larger air mass instead of being used only for evaporation. The shaded region in Figure 9 identifies the high-GOR operating window, approximately between 0.055 and 0.075 kg/s. Within this range, the system provides strong vapor transport while avoiding excessive thermal penalty from very high air circulation. Therefore, the optimum air-flow range should be selected by considering both freshwater productivity and GOR. Although Figure 8 showed that productivity continued to increase at higher air flow rates, Figure 9 demonstrates that the most energy-efficient operation occurs before the maximum air-flow limit. Overall, the results indicate that the proposed FPC–HDH system performs best when the flat plate collector supplies feedwater close to 90°C and the air mass flow rate is maintained within the high-efficiency range. Under these conditions, the system achieved a maximum GOR of approximately 2.62, confirming that Gwadar's high solar radiation and hot summer conditions can support thermally efficient HDH desalination.

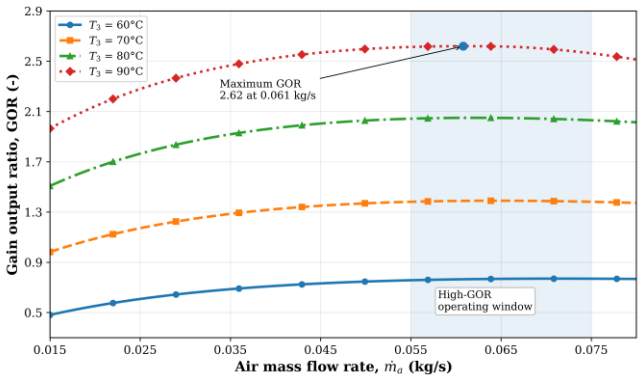

Figure 9:. Effect of air mass flow rate on gain output ratio at different humidifier inlet water temperatures.

Cooling-side performance of the dehumidifier

Figure 10 evaluates the dehumidifier's cooling-side performance by varying the coolant inlet temperature (T1) and cooling water mass flow rate ($\dot{m}_c$). In the HDH cycle, the dehumidifier removes heat from the hot, moisture-laden air leaving the humidifier. Therefore, its cooling capacity directly controls how much water vapor can condense and be collected as freshwater. Freshwater productivity increased when the coolant inlet temperature decreased. This behavior is physically expected because colder coolant provides a stronger temperature difference between the humid air stream and the cooling surface. A larger temperature difference enhances sensible cooling of the humid air and reduces the saturation humidity ratio at the dehumidifier outlet. As a result, the system removes more water vapor from the airstream and converts it into liquid freshwater. Therefore, productivity is highest at low coolant inlet temperatures, particularly near (T_1 = 24 – 28 °C). The cooling water mass flow rate also strongly influences freshwater production. At low cooling flow rates, the coolant absorbs heat rapidly, and its temperature rises significantly, weakening the condensation driving force. Increasing ($\dot{m}_c$) improves heat removal from the dehumidifier and keeps the cooling surface temperature lower. Consequently, the dehumidifier outlet air temperature decreases and the condensation rate increases. However, the contour shape also shows that the improvement weakens at higher cooling flow rates, indicating diminishing-return behavior. This occurs because once the cooling surface becomes sufficiently cold, further increase in coolant flow provides only a limited additional reduction in outlet air humidity. For the marked representative cooling condition of (T_1 = 26 °C) and ($\dot{m}_c$ = 0.065 kg/s), the freshwater productivity reached approximately 5.95 kg/h. Under these conditions, the dehumidifier outlet air temperature was about 35.9°C, while the coolant outlet temperature increased to nearly 48.6 °C. This indicates effective heat recovery from the humid air stream and confirms that adequate cooling-water circulation is essential to maintain high condensation performance. The overlaid coolant outlet temperature contours provide additional insight into heat removal. At lower cooling water mass flow rates, the coolant outlet temperature becomes higher because the same condensation and sensible heat load is absorbed by a smaller coolant stream. In contrast, increasing the cooling water flow rate reduces the coolant temperature rise and stabilizes dehumidifier operation. Therefore, the cooling flow rate should be selected carefully to balance condensation enhancement, pumping energy, and system simplicity. Overall, the results demonstrate that the dehumidifier is a key limiting component in the proposed FPC–HDH system. Even when the humidifier produces highly humid air, freshwater productivity will remain limited if the cooling side is not sufficiently effective. Under Gwadar conditions, maintaining a relatively low coolant inlet temperature and a moderate-to-high cooling water flow rate can significantly improve condensation and support freshwater production near the proposed system's favorable operating range.

NUST Journal of Engineering Sciences (NJES) is licensed under a Creative Commons Attribution 4.0 International License.

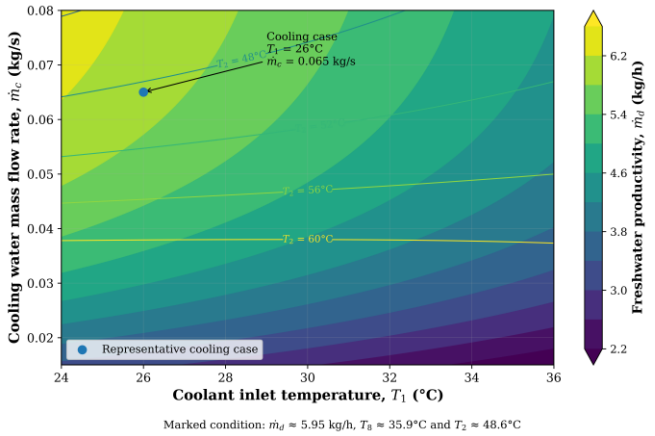

Figure 10: Effect of coolant inlet temperature and cooling water mass flow rate on freshwater productivity in the dehumidifier (Marked conditions: $\dot{m}_d$ = 5.95 kg/h, T_8 = 35.9 °C and T_2 = 48.6 °C)

Integrated hourly performance of the FPC–HDH system

The integrated hourly performance of the proposed FPC–HDH desalination system is presented in Figure 11. This analysis combines the thermal response of the flat plate collector with the humidification and dehumidification performance of the HDH unit. The hourly FPC outlet temperature was used as the humidifier inlet water temperature. Meanwhile, the air flow rate and cooling-side conditions were maintained near the favorable operating range identified in the previous sections. Freshwater productivity remained very low in the early morning because solar irradiance and FPC outlet temperature were insufficient to drive strong humidification. Between 7:00 AM and 9:00 AM, productivity increased only gradually because the humidifier inlet water temperature remained below the range required for intense evaporation. As solar radiation increased, the collector delivered higher thermal energy to the feedwater, and the HDH unit showed a rapid improvement in freshwater production. Productivity rose sharply from 10:00 AM onward as the humidifier inlet temperature exceeded the moderate-temperature range. The productivity increased from approximately 2.42 kg/h at 10:00 AM to 5.48 kg/h at 12:00 PM. Maximum freshwater productivity reached approximately 6.15 kg/h at 1:00 PM, corresponding to the highest solar input and maximum FPC outlet temperature. This confirms that the solar collector directly controls the humidifier's moisture-generation potential and, consequently, the dehumidifier's condensation rate. The GOR followed a similar trend but with a clearer peak in efficiency. It increased from low values in the morning to a maximum of approximately 2.62 around 1:00 PM. This indicates that the system used the supplied solar thermal energy most effectively during midday, when the vapor generation rate and latent heat recovery were both high. After 2:00 PM, the GOR declined because solar input and FPC outlet temperature decreased, reducing the thermal driving force for humidification. Although productivity remained relatively high at 2:00 PM, the declining GOR shows that productivity alone is not sufficient to evaluate system performance. Higher freshwater output may still be associated with lower thermal efficiency if operating conditions require more sensible heating or if heat and mass transfer become less balanced. Therefore, both productivity and GOR must be considered together when selecting the optimum operating window. The integrated freshwater yield for the selected June operating day was approximately 34.5 kg/day. Most of this production occurred between 11:00 AM and 3:00 PM, confirming that the useful operating period of the proposed solar-driven HDH system is concentrated around the high-radiation hours. These results demonstrate that Gwadar's hot summer conditions can support effective small-scale freshwater production, particularly when the FPC outlet temperature is maintained above the strong humidification range, and the dehumidifier cooling side is sufficiently effective.

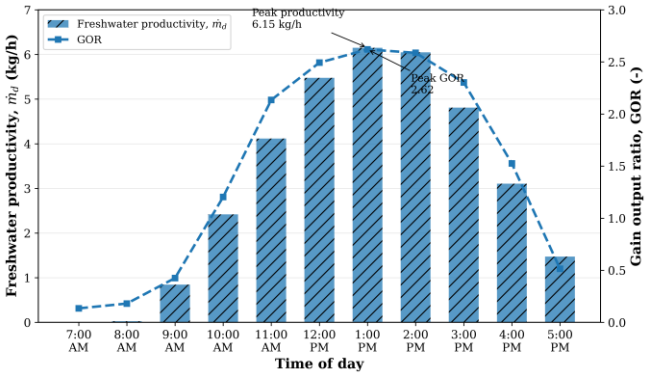

Figure 11: Integrated hourly variation of freshwater productivity and GOR for the proposed FPC–HDH desalination system under representative June operating conditions in Gwadar.

Economic Analysis of the proposed FPC–HDH system based on Pakistan

The economic sensitivity of the proposed FPC–HDH desalination system is presented in Figure 12 by evaluating the effect of annual freshwater production and capital cost on the levelized cost of water. The LCOW decreased sharply as annual freshwater production increased, showing that freshwater yield is the most influential parameter in the system's economic performance. This behavior occurs because annualized capital and maintenance costs are nearly fixed for a given system size, while produced freshwater volume varies with operating hours, solar availability, and daily productivity.

For the base capital cost of 80,000 PKR, the LCOW was approximately 18.0 PKR/L when the annual freshwater production was only 804 L/year. This represents a conservative low-production case and should not be interpreted as the system's general cost. When annual freshwater production increased to 3650 L/year (about 10 L/day), the LCOW decreased to about 4.0 PKR/L. Further improvement in annual production to 10800 L/year reduced the LCOW to nearly 1.34 PKR/L. The results also show that

NUST Journal of Engineering Sciences (NJES) is licensed under a Creative Commons Attribution 4.0 International License.

capital cost noticeably affects LCOW, especially at low annual freshwater production. At small production levels, increasing the capital cost from 60,000 to 100,000 PKR produced a large difference in water cost because the fixed annual investment was distributed over a small water output. However, as annual production increased, the difference between the low-cost, base-cost, and high-cost cases became smaller. This indicates that improving daily water yield and increasing the number of effective operating days matter more than reducing component cost alone. Overall, the economic results confirm that the proposed system becomes more attractive when it operates for longer sunshine periods and produces higher annual freshwater yield. Therefore, the LCOW should be reported as a production-dependent range rather than a single fixed value. Under the considered assumptions, system cost ranged from about 18.0 PKR/L at low production to 1.34–4.0 PKR/L under improved annual-yield conditions. This provides a more realistic economic interpretation for small-scale solar HDH desalination in Gwadar

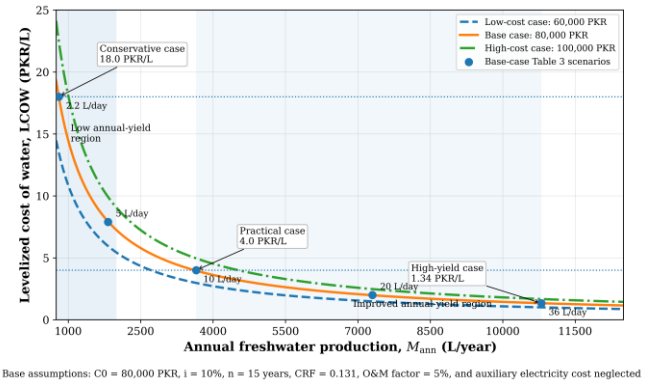

Figure 12: Sensitivity of levelized cost of water to annual freshwater production and capital cost under the considered economic assumptions.

Effect of inflation on the economic performance of the proposed FPC–HDH system

The influence of the annual inflation rate on the levelized cost of water is presented in Figure 13 for different system lifetimes. This analysis is particularly relevant for Pakistan, where inflation can strongly affect the long-term economic viability of small-scale desalination systems by increasing operating and maintenance costs over time. In the present analysis, the capital cost was fixed at 80,000 PKR, the annual freshwater production was fixed at 3650 L/year, and the first-year O&M cost was taken as 5% of the capital cost. The results show that LCOW increases continuously with increasing inflation rate for all system lifetimes. This is expected because higher inflation raises the future O&M cost and therefore increases the average annual cost of water production. At low inflation, a longer system lifetime provides an economic advantage because the capital cost is distributed over more operating years. For example, at zero inflation, the LCOW was approximately 4.66 PKR/L for a 10-year lifetime, 3.98 PKR/L for a 15-year lifetime, and 3.67 PKR/L for a 20-year lifetime. However, as inflation increases, the advantage of a longer system lifetime weakens because the cumulative escalation of annual O&M costs becomes more significant. At an inflation rate of 10%, which represents the base financial case used in this figure, the LCOW for the 15-year system increased to approximately 5.20 PKR/L. Under the same inflation rate, the 10-year and 20-year lifetime cases yielded about 5.31 PKR/L and 5.71 PKR/L, respectively. This indicates that under moderate inflation, the 15-year system provides a balanced compromise between capital recovery and long-term operating-cost escalation.

At very high inflation rates, the longer-lifetime system loses its economic advantage because compounded O&M escalation dominates the benefit of lower annualized capital cost. For example, at 25% inflation, the LCOW increased to about 7.21 PKR/L for the 10-year case, 10.90 PKR/L for the 15-year case, and more than 21 PKR/L for the 20-year case. This trend demonstrates that inflation is a critical economic factor for long-term desalination planning in developing economies. Overall, the analysis confirms that the economic performance of the proposed FPC–HDH system is not governed only by capital cost and freshwater production, but also by the macroeconomic environment. Therefore, inflation sensitivity should be considered when evaluating the practical feasibility of solar desalination systems in Pakistan, especially for long project lifetimes. The inflation sensitivity analysis may be interpreted separately from the base-case annualized-cost calculation. In the base case, the capital investment was annualized at a 10% discount rate, while the annual O&M cost was estimated as a fixed percentage of the initial capital cost. In the inflation analysis, the effect of escalating O&M expenditure was examined under different inflation-rate and plant-lifetime scenarios. For a consistent financial interpretation, nominal cash flows should be evaluated using a nominal discount rate, whereas inflation-adjusted real cash flows should be evaluated using a real discount rate. This analysis does not constitute a fully integrated discounted-cash-flow assessment that incorporates all future operating expenses, component replacements, and inflation effects simultaneously. Accordingly, the inflation results are intended to demonstrate the sensitivity of estimated water-production costs to changes in O&M expenditure and plant lifetime. They should not be interpreted as a complete life-cycle financial forecast.

Year-Round Climatic Conditions and Seasonal System Performance

The principal performance reference is the favorable summer operating condition identified in this study, where solar irradiance reaches approximately 960 W/m² and ambient temperature reaches 39.2°C. Under these conditions, the collector outlet temperature reaches approximately 90.1°C, the useful heat gain is about 0.66 kW, and the HDH system achieves a maximum freshwater productivity of 6.15 kg/h with a gain output ratio (GOR) of 2.62. These values provide a quantitative reference against which the seasonal response can be evaluated.

NUST Journal of Engineering Sciences (NJES) is licensed under a Creative Commons Attribution 4.0 International License.

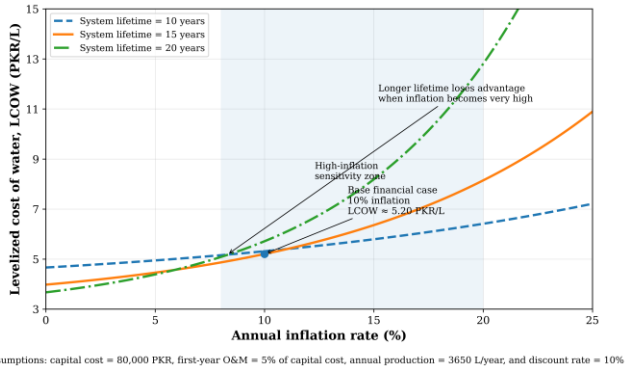

Figure 13: Sensitivity of the levelized cost of water to annual inflation rate in Pakistan for different system lifetimes under base-case capital cost, annual freshwater production, and O&M assumptions.

Climatic influence on collector performance. As shown conceptually in Figure 14(a)**,** solar irradiance is the principal time-varying energy input to the FPC. The absorbed solar energy increases the absorber-plate temperature and drives heat transfer to the circulating seawater. Under favorable summer conditions, an irradiance of 960 W/m² incident on the 1.5 m² collector aperture corresponds to an incident solar power of approximately 1.44 kW, calculated as GA_c. Compared with the reported useful heat gain of 0.66 kW, this gives an indicative useful-heat-to-incident-solar-power ratio of approximately 45.8%. This ratio is a calculated diagnostic value, not a separately validated collector efficiency; its interpretation depends on the precise definition of useful heat gain and the collector boundary conditions. The remaining incident energy is associated with optical losses, reflection, and thermal losses to the surroundings. Consequently, the collector outlet temperature does not increase in direct proportion to irradiance alone: ambient temperature, inlet-water temperature, flow rate, absorber properties, and insulation also affect the thermal balance.

The reported summer ambient temperature of 39.2°C is particularly relevant because it affects the temperature difference between the collector and its surroundings. Although a higher ambient temperature can reduce collector heat loss for a given absorber temperature, it also changes the temperature conditions of the incoming air and the HDH components. The seawater inlet temperature, which reaches approximately 34.1°C in the representative summer conditions, further influences the collector's available temperature rise. Therefore, evaluate the climatic variables together rather than treating solar irradiance as the only determinant of system performance.

Collector outlet temperature and freshwater production. Figure 14(b) links the FPC's thermal response to freshwater production. The reported collector outlet temperature of approximately 90.1°C indicates that the collector can provide a hot-water stream suitable for supplying thermal energy to the humidifier under the investigated operating conditions. Increasing the humidifier inlet-water temperature generally raises the saturation humidity of the air in contact with the heated saline water, increasing the potential for water evaporation. The resulting humid air is then cooled in the dehumidifier, where some water vapor condenses and is collected as freshwater. The actual productivity depends not only on the collector outlet temperature but also on air and water mass flow rates, humidifier and dehumidifier effectiveness, coolant inlet temperature, and the coupled heat and mass balances.

At the favorable operating point, the maximum freshwater productivity is 6.15 kg/h. If this peak rate were maintained continuously for 24 h, the corresponding production would be 147.6 kg/day. However, this is only a theoretical continuous-operation equivalent, not the actual daily yield of the solar-driven system. The manuscript reports a daily yield of approximately 34.5 kg, equivalent to about 5.61 h of production at the peak rate. This comparison shows why peak hourly productivity should not be multiplied by 24 to estimate daily production: solar irradiance varies during the day, and the system cannot be assumed to operate at peak conditions continuously.

GOR and thermal utilization. Figure 14(c) is intended to relate freshwater productivity to the GOR. The reported peak GOR of 2.62 indicates that the freshwater production, expressed on the study's adopted GOR basis, is favorable relative to the thermal energy supplied. A higher GOR generally indicates more effective use of the supplied thermal energy for evaporation and condensation. Nevertheless, GOR is not determined by collector temperature alone. Increasing the hot-water temperature may enhance evaporation, but the benefit can be limited by dehumidifier capacity, insufficient cooling, changes in flow-rate ratios, or increased thermal losses. Thus, freshwater productivity and GOR should be interpreted together: a condition that maximizes the instantaneous freshwater production does not necessarily maximize GOR under every operating configuration.

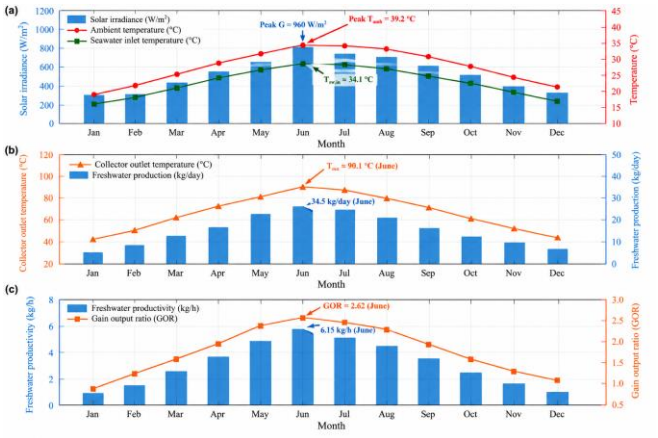

Figure 14: Climatic conditions and performance indicators for the FPC-driven HDH desalination system in Gwadar, Pakistan: (a) monthly solar irradiance, ambient temperature, and seawater inlet temperature; (b) collector outlet temperature and freshwater production; and (c) freshwater productivity and gain output ratio (GOR).

NUST Journal of Engineering Sciences (NJES) is licensed under a Creative Commons Attribution 4.0 International License.

Model Validation, RMSE, and Uncertainty Analysis

The flat plate collector (FPC) model was validated against the experimental data of Ameri and Eshaghi [13] using Zambolin's test conditions, with a water mass flow rate of 0.0427 kg/s and solar irradiance of 1000 W/m². As shown in Figure 15, the predicted outlet temperatures were 28.62°C and 90.48°C, compared with experimental values of 30.0°C and 94.8°C, respectively. The mean relative error was 4.58%, and the root mean square error (RMSE) was calculated as:

$$\mathrm{RMSE} = \sqrt{\frac{1}{N}\sum_{i=1}^{N}\left(T_{p,i} - T_{ref,i}\right)^2} \tag{44}$$

where $T_{p,i}$ and $T_{ref,i}$ represent the predicted and experimental temperatures from the references, respectively, and (N) is the number of validation points. The calculated FPC RMSE was 3.21°C, compared with the reference Ameri and Eshaghi [13]. The HDH model was validated against the water-heated cycle data of Sharqawy et al. [15], as presented in Figure 16. The model reproduced the characteristic increase and subsequent decrease in gain output ratio (GOR) with increasing mass flow rate ratio (MR). The predicted peak GOR was approximately 1.79, compared with the reference value of 1.89, while the average relative error was 4.68%. These results indicate reasonable agreement between the model predictions and reference data.

The uncertainty and sensitivity assessment is presented in Figure 17, which illustrates the estimated percentage changes in freshwater productivity and GOR associated with perturbations in the principal operating parameters. Solar irradiance and humidifier effectiveness exhibit comparatively large effects on predicted performance, whereas ambient and coolant inlet temperatures show smaller effects. This assessment highlights the importance of accurately specifying the principal thermal and operating parameters when evaluating the proposed FPC–HDH desalination system's performance.

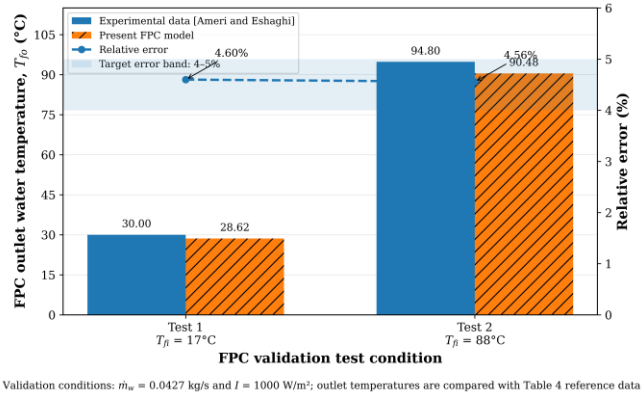

Figure 15: Validation of the present FPC model against the experimental outlet water temperature data reported by Ameri and Eshaghi using Zambolin's flat plate collector test conditions.

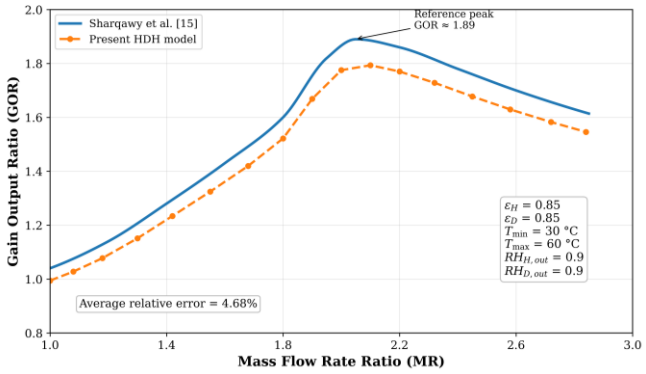

Figure 16: Validation of the HDH model with Sharqawy et al. [15]

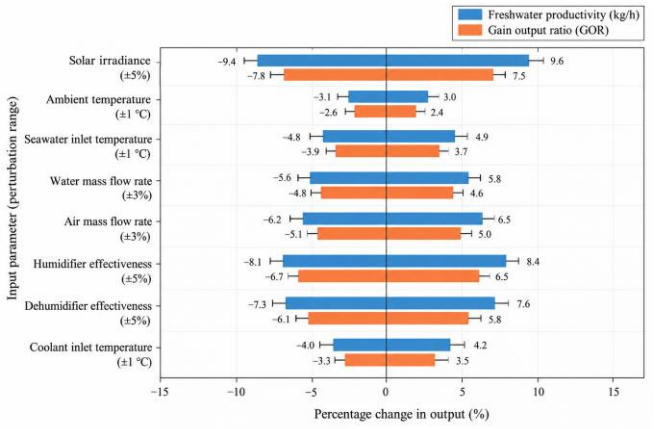

Figure 17: Sensitivity of freshwater productivity and gain output ratio (GOR) to uncertainties in the principal operating parameters of the FPC–HDH desalination system.

Interpretation of the LCOW range and comparison with alternative water supplies

The estimated LCOW range of 1.34–18.0 PKR/L reflects the proposed FPC–HDH system's sensitivity to annual freshwater production rather than a single fixed production cost. As shown in Table 4, the annualized system cost was maintained at PKR 14,480/year, while annual freshwater production varied across the considered economic scenarios. Under the conservative scenario of 804 L/year, the estimated LCOW was 18.0 PKR/L. Increasing annual production to 3,650 L/year reduced the LCOW to approximately 4.0 PKR/L, while the higher-production scenario of 10,800 L/year yielded an estimated LCOW of approximately 1.34 PKR/L. This reduction occurs because the annualized cost is distributed over a greater volume of freshwater. These values represent scenario-based economic estimates and should not be interpreted as experimentally measured costs or as proof that every production level can be sustained throughout the year. Comparing alternative water supplies requires considering differences in technology, water source, plant capacity, operating conditions, and cost boundaries. Reverse osmosis (RO) is an established desalination technology, but reported costs depend on whether the feedwater is brackish water or seawater and whether the estimate includes only operating

NUST Journal of Engineering Sciences (NJES) is licensed under a Creative Commons Attribution 4.0 International License.

expenditure or also capital recovery, pretreatment, membrane replacement, and other expenses. For example, a Pakistan-focused industry source reports operating costs of approximately PKR 70–150/m³ for brackish-water RO, equivalent to PKR 0.07–0.15/L; this figure is not directly comparable with the present LCOW because the water source and cost boundaries differ [reference to be verified and added]. Locally supplied water also has a location- and date-dependent price. Historical reporting from Gwadar documented substantial household expenditure on tanker-supplied water, while a January 2024 market-price report listed 19-L drinking-water containers at PKR 110–370, equivalent to approximately PKR 5.79–19.47/L [references to be added]. These examples illustrate why the relevant benchmark depends on whether the proposed system is compared with bulk desalinated water, tanker deliveries, or packaged drinking water. Accordingly, the present results indicate that the proposed FPC–HDH system may offer an alternative for decentralized freshwater production under favorable production conditions. Still, a definitive economic advantage over RO or locally supplied water cannot be established without a consistent comparison using current local prices and equivalent life-cycle cost boundaries.

Environmental and Ethical Considerations of Brine Disposal

Brine management is an important environmental consideration for the proposed FPC–HDH desalination system in Gwadar. Desalination brine contains concentrated dissolved salts and may also contain residual treatment chemicals or trace metals, depending on the process and materials used. Uncontrolled discharge can increase local seawater salinity and potentially affect marine organisms by disrupting their osmotic balance. Thermal differences and contaminant accumulation may further contribute to localized environmental stress. Panagopoulos et al. [24] highlighted that the environmental impact of brine discharge depends on its characteristics, discharge conditions, and the hydrodynamic properties of the receiving water body. Therefore, any practical implementation of the proposed system should adopt responsible brine management, including a suitably designed discharge arrangement, adequate dilution and mixing where direct marine discharge is permitted, and monitoring of receiving-water salinity and temperature. The discharge point should be selected to minimize impacts on sensitive marine habitats. Brine treatment, salt recovery, or zero-liquid-discharge approaches may also be considered where technically and economically feasible. Because the present study does not experimentally assess brine dispersion or marine ecological effects in Gwadar, a site-specific environmental assessment is required before implementation to ensure that freshwater production does not pose unacceptable risks to the coastal ecosystem.

Policy Implications for Decentralized Solar Desalination in Balochistan

The findings highlight the potential of solar-driven humidification–dehumidification (HDH) desalination as a decentralized freshwater production option for water-stressed coastal communities in Balochistan, particularly in Gwadar. Governmental support could facilitate its adoption through targeted capital subsidies, concessional financing, and pilot demonstration projects for small-scale solar desalination systems. Collaboration among provincial water authorities, local governments, universities, and private-sector stakeholders could support technology deployment, local technical training, and long-term operation and maintenance. Incentives could also encourage locally manufactured components and community-managed desalination units, reducing dependence on centralized water supply and costly water transportation. However, financial support should be linked to demonstrated technical performance, freshwater quality standards, sustainable brine management, and transparent operating costs. Pilot projects and site-specific assessments are therefore recommended before large-scale deployment to establish the system's suitability, affordability, and environmental acceptability under local conditions.

Conclusion

Gwadar's climatic conditions are favorable for solar-driven HDH desalination due to high solar radiation, hot ambient temperatures, and direct seawater availability. On the representative June day, solar irradiance reached approximately 960 W/m², providing strong thermal input to the flat plate collector.

The major findings of this study are summarized as follows:

- The FPC outlet temperature increased to about 90.1°C, while the useful heat gain reached nearly 0.66 kW. This confirms that the flat plate collector can provide sufficiently hot feedwater for the humidifier during peak solar hours.
- Collector material selection had a clear effect on thermal performance. Copper produced the highest outlet temperature, followed by aluminum and steel. Aluminum may be considered a cost-effective alternative, whereas steel is less suitable because of its lower thermal conductivity.
- Polyurethane insulation performed better than mineral wool because of its lower bottom heat-loss coefficient. This helped maintain a higher collector outlet temperature and improved thermal delivery to the HDH unit.
- The HDH subsystem was strongly affected by humidifier inlet water temperature, air mass flow rate, and dehumidifier cooling conditions. Under favorable operating conditions, the maximum freshwater productivity reached approximately 6.15 kg/h, while the peak GOR reached about 2.62.
- The integrated freshwater yield for the selected June operating day was approximately 34.5 kg/day. Most freshwater production occurred between 11:00 AM and

NUST Journal of Engineering Sciences (NJES) is licensed under a Creative Commons Attribution 4.0 International License.

3:00 PM, showing that the system performs best during the high-radiation period.

- The economic analysis showed that LCOW is highly dependent on annual freshwater production. For a base capital cost of 80,000 PKR, LCOW was about 18.0 PKR/L under conservative low-yield operation, but fell to about 4.0 PKR/L at 10 L/day and nearly 1.34 PKR/L under improved annual-yield operation.
- Inflation sensitivity is an important finding for Pakistan. At low inflation, longer system lifetime improves cost performance by spreading the capital cost over more years. However, under high inflation, operation and maintenance costs increase significantly and can reduce the economic advantage of longer project life.
- At 10% inflation, the 15-year system lifetime provided a balanced LCOW of approximately 5.20 PKR/L. However, very high inflation sharply increased water costs, especially for longer system lifetimes. Therefore, practical deployment in Pakistan should consider inflation, maintenance escalation, realistic annual productivity, and not only the initial capital cost.

Overall, the proposed solar-driven FPC–HDH desalination system is technically feasible and economically promising for decentralized freshwater production in Gwadar and similar arid coastal regions. Its simple configuration, solar operation, and suitability for small coastal communities make it a practical option where seawater is available but freshwater access is limited. Future work should focus on experimentally validating the proposed FPC–HDH system using a laboratory-scale prototype and investigating its integration with hybrid solar-energy systems to improve freshwater productivity, energy utilization, and operational reliability.

Competing Interests

The authors declare no known competing financial interests or personal relationships that could have appeared to influence the work reported in this manuscript.

Funding Statement

This research received no specific grant from any funding agency in the public, commercial, or not-for-profit sectors.

Ethical Statement

This study did not involve any human participants, human data, animals, or animal-derived materials. Therefore, ethical approval was not required.

Declaration of AI Use

During the preparation of this manuscript, AI-based tools were used only for grammar refinement, structural improvement, and enhancement of figure/image quality. The authors developed and verified the scientific content, methodology, interpretation of results, and conclusions.

Data Availability Statement

The data supporting the findings of this study are available from the corresponding author upon reasonable request.

References

1. Systems. G, “The Water Crisis”, 2016. Available from: https://genesissystems.com/the-water-crisis/4. Accessed: 10 September 2023.
2. Santosh. R et al., “Technological advancements in solar energy driven humidification-dehumidification desalination systems-A review”, Journal of Cleaner Production, Vol. 207, 2019, pp. 826-845.
3. Mohamed. A.I and El-Minshawy. N, “Theoretical investigation of solar humidification–dehumidification desalination system using parabolic trough concentrators”, Energy Conversion and Management, Vol. 52, No. 10, 2011, pp. 3112-3119.
4. Khalil. A et al., “Solar water desalination using an air bubble column humidifier”, Desalination, Vol. 372, 2015, pp. 7-16.
5. Yıldırım. C and Solmuş. İ, “A parametric study on a humidification–dehumidification (HDH) desalination unit powered by solar air and water heaters”, Energy Conversion and Management, Vol. 86, 2014, pp. 568-575.
6. Sharshir. S et al., “A hybrid desalination system using humidification-dehumidification and solar stills integrated with evacuated solar water heater”, Energy Conversion and Management, Vol. 124, 2016, pp. 287-296.
7. Antar. M.A and Sharqawy. M.H, “Experimental investigations on the performance of an air heated humidification–dehumidification desalination system”, Desalination and Water Treatment, Vol. 51, No. 4-6, 2013, pp. 837-843.
8. Dai. Y, Wang. R and Zhang. H, “Parametric analysis to improve the performance of a solar desalination unit with humidification and dehumidification”, Desalination, Vol. 142, No. 2, 2002, pp. 107-118.
9. Dai. Y and Zhang. H, “Experimental investigation of a solar desalination unit with humidification and dehumidification”, Desalination, Vol. 130, No. 2, 2000, pp. 169-175.
10. Zhani. K and Bacha. H.B, “Experimental investigation of a new solar desalination prototype using the humidification dehumidification principle”, Renewable Energy, Vol. 35, No. 11, 2010, pp. 2610-2617.
11. Kabeel. A and El-Said. E.M, “A hybrid solar desalination system of air humidification–dehumidification and water flashing evaporation: Part I. A numerical investigation”, Desalination, Vol. 320, 2013, pp. 56-72.
12. Yamalı. C and Solmuş. İ, “Theoretical investigation of a humidification-dehumidification desalination system configured by a double-pass flat plate solar air heater”, Desalination, Vol. 205, No. 1-3, 2007, pp. 163-177.

NUST Journal of Engineering Sciences (NJES) is licensed under a Creative Commons Attribution 4.0 International License.

13. Ameri. M and Eshaghi. M.S, "A novel configuration of reverse osmosis, humidification–dehumidification and flat plate collector: Modeling and exergy analysis", Applied Thermal Engineering, Vol. 103, 2016, pp. 855-873.
14. Duffie. J.A and Beckman. W.A, "Solar engineering of thermal processes", John Wiley & Sons, 2013.
15. Sharqawy. M.H et al., "Optimum thermal design of humidification dehumidification desalination systems", Desalination, Vol. 349, 2014, pp. 10-21.
16. Chehayeb. K.M, Narayan. G.P and Zubair. S.M, "Use of multiple extractions and injections to thermodynamically balance the humidification dehumidification desalination system", International Journal of Heat and Mass Transfer, Vol. 68, 2014, pp. 422-434.
17. Organization. W.H, "Guidelines for drinking-water quality: first addendum to the fourth edition", 2017.
18. Sharqawy. M.H, Lienhard. J.H and Zubair. S.M, "Thermophysical properties of seawater: a review of existing correlations and data", Desalination and Water Treatment, Vol. 16, No. 1-3, 2010, pp. 354-380.
19. Hermosillo. J.-J, Arancibia-Bulnes. C.A and Estrada. C.A, "Water desalination by air humidification: Mathematical model and experimental study", Solar Energy, Vol. 86, No. 4, 2012, pp. 1070-1076.
20. Hamed. M.H et al., "Mathematical and experimental investigation of a solar humidification–dehumidification desalination unit", Desalination, Vol. 358, 2015, pp. 9-17.
21. Al-Sahali. M and Ettouney. H.M, "Humidification dehumidification desalination process: Design and performance evaluation", Chemical Engineering Journal, Vol. 143, No. 1-3, 2008, pp. 257-264.
22. Al-Sulaiman. F.A et al., "Humidification dehumidification desalination system using parabolic trough solar air collector", Applied Thermal Engineering, Vol. 75, 2015, pp. 809-816.
23. Somwanshi. A and Sarkar. N, "Thermal performance of a dual-purpose collector-cum-storage type air-water heater", Applied Thermal Engineering, Vol. 171, 2020, pp. 115094.
24. Panagopoulos. A, Haralambous. K.J and Loizidou. M, "Desalination brine disposal methods and treatment technologies - A review", Science of the Total Environment, Vol. 693, 2019, pp. 133545. https://doi.org/10.1016/j.scitotenv.2019.07.351



NUST Journal of Engineering Sciences (NJES) is licensed under a Creative Commons Attribution 4.0 International License.